



ELSEVIER

Available online at [www.sciencedirect.com](http://www.sciencedirect.com)

SCIENCE @ DIRECT®

Physica D 179 (2003) 33–52

PHYSICA D

[www.elsevier.com/locate/physd](http://www.elsevier.com/locate/physd)

# Analogy between a 10D model for nonlinear wave–wave interaction in a plasma and the 3D Lorenz dynamics

C. Letellier<sup>a,\*</sup>, L.A. Aguirre<sup>b</sup>, J. Maquet<sup>a</sup>, B. Lefebvre<sup>c</sup>

<sup>a</sup> CORIA/CNRS UMR 6614, Université de Rouen, Av. de l'Université, BP 12, F-76801 Saint-Etienne du Rouvray Cedex, France

<sup>b</sup> Universidade Federal de Minas Gerais, Av. Antônio Carlos 6627, 31.270-901 Belo Horizonte, MG, Brazil

<sup>c</sup> LPCE/CNRS UMR 6115, Université d'Orléans, 3A Av. de la Recherche Scientifique, F-45071 Orléans, France

Received 17 July 2002; received in revised form 19 November 2002; accepted 18 December 2002

Communicated by C.K.R.T. Jones

## Abstract

This paper investigates nonlinear wave–wave interactions in a system that describes a modified decay instability and consists of three Langmuir and one ion-sound waves. As a means to establish that the underlying dynamics exists in a 3D space and that it is of the Lorenz-type, both continuous and discrete-time multivariable global models were obtained from data. These data were obtained from a 10D dynamical system that describes the modified decay instability obtained from Zakharov's equations which characterise Langmuir turbulence. This 10D model is equivariant under a continuous rotation symmetry and a discrete order-2 rotation symmetry. When the continuous rotation symmetry is modded out, that is, when the dynamics are represented with the continuous rotation symmetry removed under a local diffeomorphism, it is shown that a 3D system may describe the underlying dynamics. For certain parameter values, the models, obtained using global modelling techniques from three time series from the 10D dynamics with the continuous rotation symmetry modded out, generate attractors which are topologically equivalent. These models can be simulated easily and, due to their simplicity, are amenable for analysis of the original dynamics after symmetries have been modded out. Moreover, it is shown that all of these attractors are topologically equivalent to an attractor generated by the well-known Lorenz system.

© 2003 Elsevier Science B.V. All rights reserved.

PACS: 05.45.+b

Keywords: Wave–wave interaction; Plasma; 3D Lorenz dynamics

## 1. Introduction

Parametric processes and nonlinear interaction between waves play a basic role near the onset of numerous plasma instabilities. Due to its relative simplicity, richness of nonlinear regimes and applications to both space and laboratory plasmas [1], Langmuir turbulence provides an attractive framework for studies of parametric instabilities. Furthermore, there are some observational evidences for the occurrence of such parametric instabilities involving only a few Langmuir waves, e.g. in the solar wind [2–5]. These may arise when the linear instability growth rate is

\* Corresponding author.

E-mail address: [christophe.letellier@coria.fr](mailto:christophe.letellier@coria.fr) (C. Letellier).

relatively small, and when non-resonant and secondarily excited waves are sufficiently damped. Finding appropriate descriptions of the involved dynamics and developing relevant data analysis techniques are important problems that are not quite solved.

Since the underlying dynamics is characterised by a low-dimensional chaotic attractor, the nonlinear dynamical system theory provides rather powerful techniques to describe the dynamical properties of such instability. A few of them like the correlation dimension and Lyapunov exponents have already been used [6]. These geometrical invariants confirm the low-dimensionality of the dynamics but do not reveal much about the mechanisms responsible for the structure of the associated attractor. Typically, chaotic behaviour results from stretching and folding processes. Stretching ensures the sensitivity to initial conditions and boundedness of the attractor requires folding. In the most favourable cases, both may be described using a branched manifold that synthesises the topological properties of the unstable periodic orbits [7]. These periodic orbits are the skeleton of the chaotic attractor. Indeed, the chaotic trajectory evolves among these orbits. The key point is that investigating the relative organisation of the low-periodic orbits is sufficient to identify most of topological properties of the chaotic trajectory. Moreover, since only the low periodic orbits are taken into account, such analysis is more robust against noise contamination than techniques based on geometrical considerations.

Another important task when one is dealing with experimental data is to obtain a set of equations that capture the underlying dynamics. The obtained model may be built using delay coordinates [8] or derivative coordinates [9]. In the former case, the model is discrete in time whilst the latter is continuous in time. The equations are therefore discrete maps or ordinary differential equations. In both cases, iterating or integrating the global model produces “synthetic data” on a chaotic attractor that is, if the models are dynamically valid, topologically equivalent to the attractor reconstructed from the experimental data. Therefore the obtained models are validated using topological analysis [10]. Both modelling techniques will be here illustrated.

In this paper, we shall perform a topological analysis and global modelling of the system of interacting electrostatic waves considered in [6,11], which involves Langmuir and ion-sound modes. This system is the simplest which, depending on the parameters, can describe two basic instabilities, namely decay and modified decay. This will provide an example of how these modelling techniques may be used to characterise such dynamics.

In particular, we shall investigate the consequences of symmetry, which is a quite generic a property for this type of systems. When a dynamical system exhibits symmetry properties, it is useful to modd them out in order to perform a more convenient dynamical analysis. That is, the data are transformed to yield a representation of the dynamics without any residual symmetry but that is locally diffeomorphically equivalent to the original system. First, it is shown [12,13] that the dynamical analysis is significantly simplified and, second, that the physical processes are invariant under these symmetry properties. A dynamical system equivariant under symmetry properties may be understood as the cover of an image system which provides a representation without any residual symmetry [14]. The image system is locally equivalent to the cover. In fact, there is a singular set where the correspondence between the image system and the cover is not defined. This singular set allows to modd out the symmetry properties. In this paper, we will establish that the dynamics underlying the 10D model for the nonlinear wave–wave interaction in a system consisting of three Langmuir and one ion-sound waves [6] is of the Lorenz type [15] when the continuous rotation symmetry is modded out.

The subsequent part of this paper is organised as follows. The 10D model is introduced in Section 2. In order to establish the analogy between the 10D model and the Lorenz system, we take the following steps. First the procedure for modding out the continuous rotation symmetry without destroying the discrete order-2 rotation symmetry is explained. A simplified embedding of the chaotic attractor is thus obtained. Second the topological analysis of this reduced dynamics is performed in a 3D space and in the space associated with the image system which has no residual symmetry. Third, a 3D (multivariable) nonlinear auto-regressive moving average (NARMA) model is obtained for this dynamics. Fourth, the NARMA model is validated using a topological analysis of the image

system. Similar results are obtained with a continuous-time model. Fifth, a topological comparison between the reduced dynamics reproduced by the 3D global models and the 3D Lorenz system is discussed. Each of these steps is described in some detail in the subsections of [Section 3](#). [Section 4](#) gives the conclusion.

## 2. The model

Langmuir turbulence is accurately described by Zakharov's equations [16]

$$\nabla \cdot (i\partial_t + \Delta + i\tilde{\nu}E) = \nabla \cdot nE, \quad (\partial_t^2 + 2\tilde{\nu}_S\partial_t - \Delta)n = \Delta|E|^2, \quad (1)$$

where  $E$  is the electric field averaged over the plasma frequency  $\omega_p$ ,  $n$  the quasi-neutral density fluctuations and  $\nu$  represents linear (Landau) damping and growth rates. Similar equations exist in the presence of a weak magnetic field [17]. These equations display a very rich variety of solutions. In this paper, the case considered in [6,11] of a 1D spectrum truncated to four waves is investigated. Such a model is the simplest which allows for two kinds of parametric instabilities of basic importance for Langmuir turbulence: decay or modified decay instabilities. The model is obtained from Zakharov equations by taking the following ansatz:

$$E = \sum_{j=1}^3 a_j(t) e^{i(k_j x - \omega_j t)} + \text{c.c.}, \quad n = b(t) e^{i(\kappa x - \Omega t)} + \text{c.c.} \quad (2)$$

with  $\omega_1 > \omega_2 > \omega_3 > 0$ ,  $\omega_j = \omega(k_j)$ , and the resonance conditions

$$(\Omega + \omega_2 - \omega_1, \kappa + k_2 - k_1) = (\Delta, 0), \quad (\Omega + \omega_3 - \omega_2, \kappa + k_3 - k_2) = (\delta, 0) \quad (3)$$

with  $\delta, \Delta \ll \omega_i$  (later on we shall take  $\Delta = \delta = 0$ ). Under this hypothesis, the first Zhakharov equation for Langmuir waves yields (using a convenient normalisation):

$$\dot{a}_1 = -\nu_1 a_1 + a_2 b e^{-i\Delta t}, \quad \dot{a}_2 = -\nu_2 a_2 - a_1 b e^{i\Delta t} + a_3 b e^{-i\Delta t}, \quad \dot{a}_3 = -\nu_3 a_3 - a_2 b^* e^{i\delta t}, \quad (4)$$

while the second-order equation for the ion-sound wave can be written as

$$\dot{b} = -2\nu_0 b + 2i(b - c), \quad \dot{c} = -\nu_0 b - a_1 a_2^* e^{-i\Delta t} - a_2 a_3^* e^{-i\delta t}. \quad (5)$$

In order to simplify the notation in the subsequent part of this paper, we will designate mode  $b$  by  $a_4$  and mode  $c$  by  $a_5$ . Depending on which mode is excited, the system (4) and (5) describes either a cascade of two decay instabilities as  $L_1 \rightarrow L_2 + S$  (L standing for Langmuir and S for ion-sound) and  $L_2 \rightarrow L_3 + S$  or modified decay instability as  $L_2 + L_2 \rightarrow L_1 + L_3$ . The second-order equation for the ion-sound should be maintained since modified decay instability has a linear growth rate of the order of  $\Omega$  [18].

When  $\Delta = \delta = 0$ , the system (4) and (5) is a nonlinear dynamical system in

$$\mathbb{C}^5(a_k) = \mathbb{R}^{10}(x_k, y_k) \quad \text{with } k = 1, 2, \dots, 5$$

which is dissipative when the trace of its Jacobian matrix  $-2(2\nu_0 + \nu_1 + \nu_2 + \nu_3)$  is negative. This is a requirement for instability saturation. These equations are equivariant under the two parameter group of rotations generated by

$$G_{\theta_1, \theta_2} : \begin{bmatrix} a_1 \\ a_2 \\ a_3 \\ a_4 \\ a_5 \end{bmatrix} \mapsto \begin{bmatrix} a_1 e^{i\theta_1} \\ a_2 e^{i\theta_2} \\ a_3 e^{i(2\theta_2 - \theta_1)} \\ a_4 e^{i(\theta_1 - \theta_2)} \\ a_5 e^{i(\theta_1 - \theta_2)} \end{bmatrix} \quad (6)$$

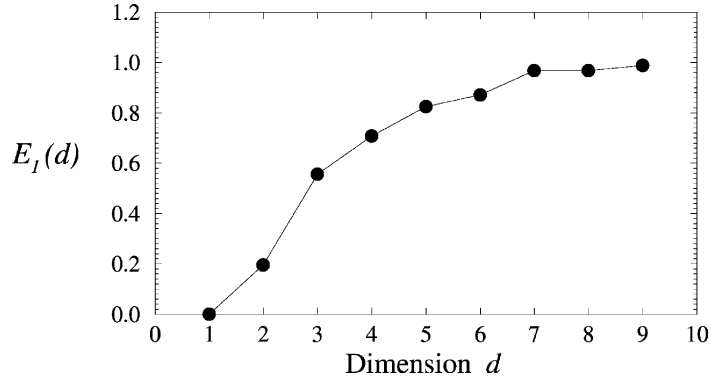


Fig. 1. Embedding dimension of the chaotic attractor generated by the 10D system. The dimension is computed by using an adapted false nearest neighbor method. In this method, the ordinates saturate when the embedding dimension is large enough. Index  $E_I(d)$  measures the relative change in the average distance between two neighbor points in  $\mathbb{R}^d$  and their respective images in  $\mathbb{R}^{d+1}$  when the dimension is increased from  $d$  to  $d+1$ . In order to do that, the phase space is reconstructed from the  $x_2$  variable using the delay coordinates with a delay  $\tau = 5.0$  s ( $\nu_1 = 0.050$ ,  $\nu_2 = -0.0345$ ,  $\nu_3 = 0.03$  and  $\nu_4 = 0.05$ ).

which defines a continuous rotation symmetry. Consequently, when using polar coordinates  $a_k = u_k e^{i\phi_k}$  ( $k = 1, \dots, 5$ ), phases appear only as linear combinations  $\Phi = \phi_4 + \phi_2 - \phi_1 - \Delta t$ ,  $\Psi = \phi_4 + \phi_3 - \phi_2 - \delta t$  and  $\Theta = \phi_4 - \phi_5$ . These phase differences represent mismatches in the resonance conditions (3) due to nonlinear interactions. The 10D system (4) and (5) may thus be reduced to an autonomous system lying in a phase space  $\mathbb{R}^8$  [6]. Nevertheless, such an approach modds out the continuous rotation symmetry, as well as the discrete order-2 symmetry. Indeed, the 10D system is equivariant under the order-2 discrete symmetry defined by the  $5 \times 5$   $\Gamma$ -matrix such as

$$\begin{bmatrix} a_1 \\ a_2 \\ a_3 \\ a_4 \\ a_5 \end{bmatrix} \mapsto \begin{bmatrix} 1 & 0 & 0 & 0 & 0 \\ 0 & -1 & 0 & 0 & 0 \\ 0 & 0 & 1 & 0 & 0 \\ 0 & 0 & 0 & -1 & 0 \\ 0 & 0 & 0 & 0 & -1 \end{bmatrix} \begin{bmatrix} a_1 \\ a_2 \\ a_3 \\ a_4 \\ a_5 \end{bmatrix} \quad (7)$$

acting on the complex modes  $a_i$ . This is an order-2 symmetry since  $\Gamma^2 = \mathbb{I}$ , where  $\mathbb{I}$  is the identity matrix. Map  $\Gamma$  then defines a discrete order-2 symmetry which is a rotation  $\mathcal{R}(\pi)$  since some of the coordinates of the phase space  $\mathbb{C}^5(a_k)$  are left invariant. It is therefore more convenient to keep the full system.

Although the phase space is 10D, the dynamics settles down onto a manifold which may be embedded in a space with a smaller dimension. Such *embedding dimension* is estimated using the false nearest neighbors technique [19]. A modified version of this technique is used here [20]. In fact the dynamics may be embedded within a 7D phase space (Fig. 1) when all symmetry properties are preserved.

A reasonable range for parameter values is  $10^{-3} \leq \nu_i \leq 10^{-1}$  according to the normalisation used, since one must have  $|\nu_i| \ll \omega_i$ . Moreover, the growth rate shall be strong enough to generate nonlinear coherent behaviour, but dissipation should quickly balance the energy input in order to prevent the formation of wideband spectra formed by a cascade of secondary instabilities. As a further restriction on the parameter range, it is worth noting that when  $\nu_1 - \nu_3 \rightarrow 0^+$ , the fixed point of the system is ejected to infinity and the approximation used for this model is no longer valid.

### 3. Dynamical analysis of the underlying dynamics

This section presents the procedure to modd out the continuous rotation symmetry from the original dynamics but preserving the order-2 discrete rotation symmetry. This order-2 rotation symmetry belongs to the symmetry group of the continuous rotation symmetry. To the best of our knowledge, it is not possible to modd out the continuous rotation in preserving the discrete one using the standard analytical procedure and this has to be done numerically as detailed below. Preserving the discrete rotation is particularly important because when the discrete rotation is modded out too, the trajectory (see Fig. 7 in [6]) is not differentiable at some points of the phase space. This becomes a problem when a global model is attempted from such reduced dynamics. Indeed, it is not possible to find a global model for this representation of the dynamics. Contrary to this, when the discrete order-2 rotation symmetry is preserved, it is possible to obtain a 3D global model using a NARMA technique or continuous-time approach as detailed in this section. The dynamics generated by these global models is topologically equivalent to the 3D embedding obtained when the continuous rotation symmetry is modded out. As it will be discussed such dynamics are of the Lorenz-type. In particular, the reduced dynamics, the global models and the Lorenz system have the same image system without any residual symmetry. A schematic diagram of all the descriptions used in the subsequent part of this paper is shown in Fig. 2.

#### 3.1. Modding out the continuous rotation

Let us investigate the modified decay investigated in [6], that is, for which the unstable mode (here mode  $L_2$ ) generates its Stokes and anti-Stokes satellites (here modes  $L_1$  and  $L_3$ ). In our notation we have  $\nu_2 < 0$  and  $\nu_0, \nu_1,$  and  $\nu_3 > 0$ . The continuous rotation symmetry as well as the order-2 discrete symmetry may be identified in plane projections of the chaotic attractor generated by the 10D system (4) and (5) (Fig. 3). Each plane projection corresponds to a mode  $a_i$ . The continuous rotation symmetry is organised around an axis which is transverse to each plane (Fig. 3) and crosses these planes at the origin. Depending on the pulsation of the modes, the rotation can become faster or slower. The modes may be ordered as  $a_1$  (fastest),  $a_2, a_4, a_5$  and  $a_3$  (slowest). Among these five

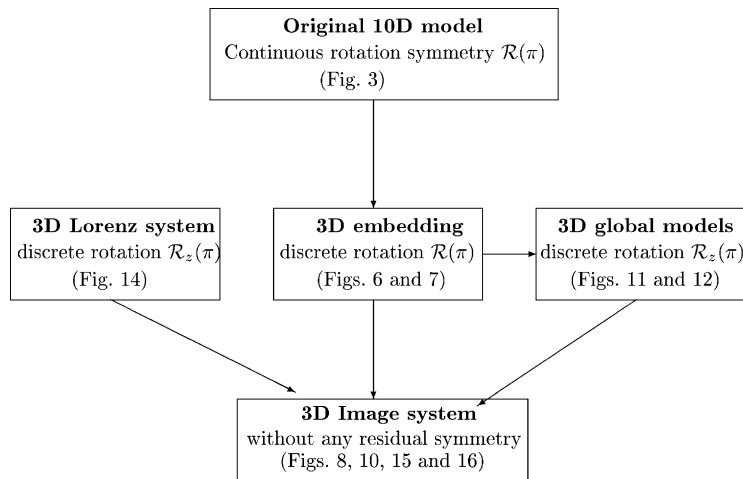


Fig. 2. Schematic diagram for the relationships between the different representation of the dynamics. From the 10D model, a 3D embedding is obtained when the continuous rotation symmetry is modded out. From this embedding, two global models are obtained. The 3D embedding, the global models and the Lorenz system ( $R = 198, \sigma = 10, b = 8/3$ ) are topologically equivalent. When the discrete rotation  $\mathcal{R}(\pi)$  is also modded out from these three representations, the three image systems continue to be topologically equivalent.

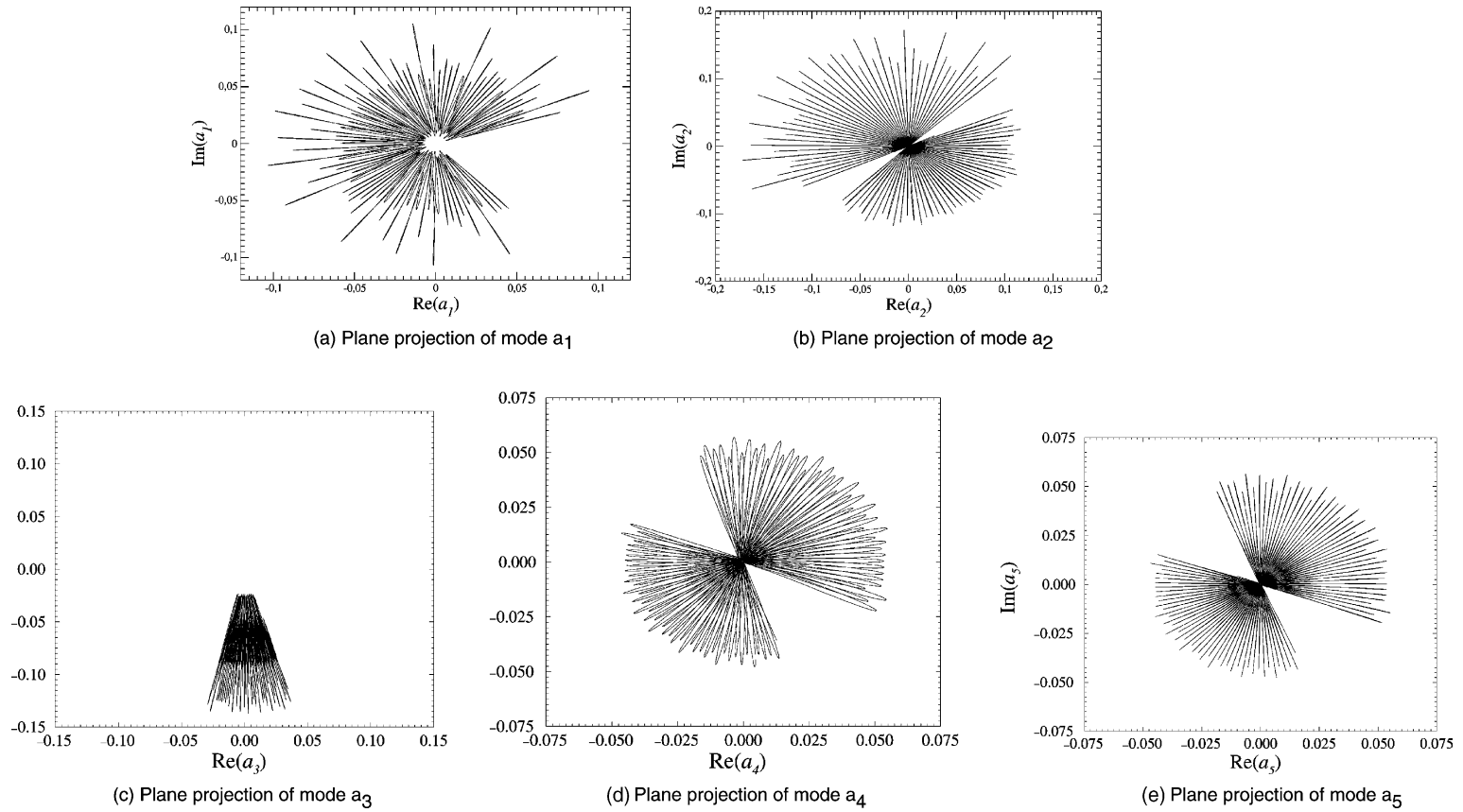


Fig. 3. Plane projections of the chaotic attractor generated by the 10D system (4) and (5). The continuous rotation symmetry is easily identified ( $\nu_1 = 0.050$ ,  $\nu_2 = -0.0345$ ,  $\nu_3 = 0.03$  and  $\nu_4 = 0.05$ ).

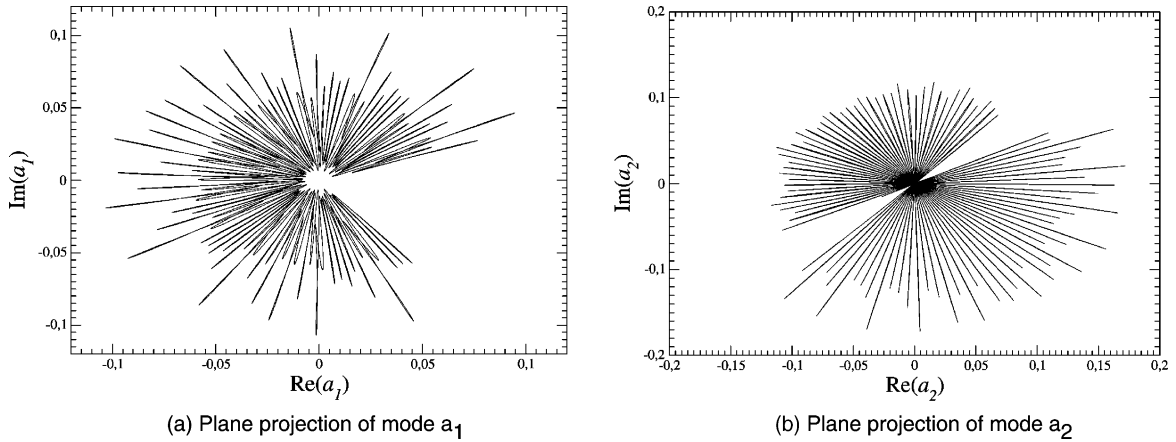


Fig. 4. Plane projections of the chaotic attractor generated by the 10D system (4) and (5) from initial conditions changed under the action of the  $\Gamma$ -matrix. Mode  $a_1$  (a) is unchanged (to compare with Fig. 3a) while mode  $a_2$  is mapped to its opposite (to compare with Fig. 3b) ( $\nu_1 = 0.050$ ,  $\nu_2 = -0.0345$ ,  $\nu_3 = 0.03$  and  $\nu_4 = 0.05$ ).

modes, only two of them  $a_1$  and  $a_3$  do not present additional oscillations around the rotation axis. Indeed, modes  $a_1$  and  $a_3$  (Fig. 3a and c) do not alternate from one side to the other of the continuous rotation axis.

These additional alternances induce the existence of the order-2 discrete rotation symmetry. Indeed, mode  $a_1$  exhibits always a large amplitude oscillation followed by a smaller amplitude oscillation (Fig. 3a). These alternance is strongly related to the alternance of oscillations of mode  $a_2$  (for instance) from one side to the other of the rotation axis (Fig. 3b). Moreover, when the initial conditions of modes  $a_2$ ,  $a_3$  and  $a_5$  are changed to their opposite, a second attractor, symmetric from the first one under the action of the  $\Gamma$ -matrix, is thus obtained. Two easily distinguishable attractors therefore coexist in the phase space (Fig. 4a and b). As expected, modes  $a_1$  and  $a_3$  are invariant under the action of the  $\Gamma$ -matrix while the three others are mapped to their opposite with respect to the rotation axis. The key point is that it is possible to map modes  $a_2$ ,  $a_3$  and  $a_5$  to their opposite while modes  $a_1$  and  $a_2$  are unchanged. This clearly indicates that two different attractors are coexisting in the phase space  $\mathbb{R}^{10}(a_1, a_2, a_3, a_4, a_5)$ . Such a feature is a strong signature of an order-2 rotation symmetry. Consequently, the alternance of the trajectory from one side to the other of the rotation axis is a signature of the second symmetry which is an order-2 discrete rotation symmetry belonging to the symmetry group of the continuous rotation symmetry. This symmetry is related to the  $\Gamma$ -matrix of relation (7).

Note that the order-2 rotation symmetry is not anymore active when the standard analytical procedure is applied since  $\Gamma$  is one of the rotation symmetry group operations. Since, up-to-now, no analytical method has been identified for doing that, a numerical procedure will be introduced as follows. The purpose is now to modd out only the continuous rotation symmetry and to preserve the discrete rotation symmetry. Usually, when a continuous rotation symmetry acting on complex modes  $a_k$  is modded out, the modulus of each mode  $a_k$  is computed according to

$$\rho_k = \pm \sqrt{|a_k|^2}. \quad (8)$$

Unfortunately, this is not only the continuous rotation symmetry which is modded out when such a coordinate transformation is applied. Indeed, when the modulus of mode  $a_k$  are computed, the discrete order-2 symmetry is also modded out. That is the reason for which the trajectory presents some point where it is not differentiable anymore (Fig. 7 in [6]). In order to preserve the discrete symmetry it is necessary to keep the phase, represented by the sign before the square root of Eq. (8). Thus the sign is changed each time the trajectory crosses the neighborhood of the rotation axis, that is the neighborhood of the trivial fixed point of the system located at the origin of the phase

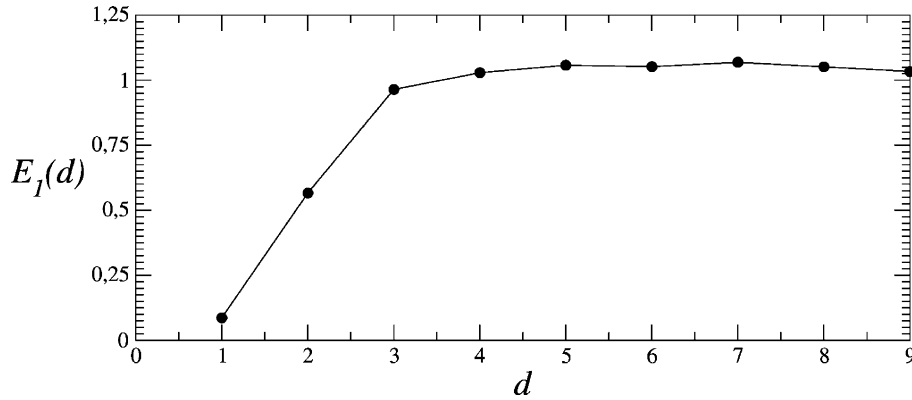


Fig. 5. Estimation of the embedding dimension from the variable  $\rho_3$ . A 3D space is clearly sufficient to describe the dynamics when the continuous rotation is removed.

space  $\mathbb{R}^{10}$ . A phase portrait which is everywhere differentiable is thus obtained (Fig. 6a). This is done for the three modes  $\rho_2$ ,  $\rho_4$  and  $\rho_5$  which are then designated by  $\tilde{\rho}_2$ ,  $\tilde{\rho}_4$  and  $\tilde{\rho}_5$ . When the continuous rotation symmetry is modded out according to Eq. (8), the phase space is obviously reduced to a 5D phase space  $\mathbb{R}^5$ . Nevertheless, the phase portrait (Fig. 6a) and its first-return map which is unimodal with a differentiable maximum (Fig. 6b) strongly suggest that the dynamics could be embedded within a 3D phase space. This is easily checked by estimating the embedding dimension using the variable  $\rho_3$  (Fig. 5).

The description of the dynamics can therefore be done in a 3D sub-space of the space  $\mathbb{R}^5(\rho_1, \tilde{\rho}_2, \rho_3, \tilde{\rho}_4, \tilde{\rho}_5)$ . Note that in this space, the  $\Gamma$ -matrix is still active as required. According to the  $\Gamma$ -matrix, there are two co-existing attractors in the phase space  $\mathbb{R}^5(\rho_1, \tilde{\rho}_2, \rho_3, \tilde{\rho}_4, \tilde{\rho}_5)$ , one is the symmetric of the other under the action of the  $\Gamma$ -matrix. In fact, two simultaneous period-doubling cascades are observed after a pitchfork bifurcation as observed for the simple Burke and Shaw system [12], and the Lorenz system. Note that when the 8D model is obtained [6], since all symmetries are modded out, the pitchfork bifurcation cannot be observed anymore and is replaced with a period-doubling bifurcation [21]. Preserving the discrete rotation allows to preserve the pitchfork bifurcation.

The chaotic attractor generated when only the continuous rotation is modded out is very similar to the chaotic attractor generated by the Lorenz system for large values of  $R$  (see Section 3.5). For instance, for the parameter values used in Fig. 6, the first-return map to a Poincaré section is a unimodal map with a differentiable maximum. Such a map belongs to the universal class associated with a period-doubling cascade [22,23] and, consequently, corresponds to the type of attractor observed for the Lorenz system for large values of  $R$  [24]. If all parameters are kept constant at the values used for Fig. 6 with the exception of  $\nu_2$ , an attractor merging crisis is observed for slightly smaller values of  $\nu_2$  and the attractor becomes globally invariant under the  $\Gamma$ -matrix (Fig. 7). A similar scenario is also observed on the Lorenz system for large values of  $R$  (see Section 3.5) and the Burke and Shaw system [13].

### 3.2. Topological analysis of the reduced dynamics

Since the attractor is now symmetric under an order-2 rotation symmetry, it is convenient to investigate its topology using the image system [14]. Indeed, a representation of the chaotic attractor without any residual symmetry may be obtained by using a  $2 \mapsto 1$  mapping. Since the attractor may be embedded within a 3D space, three coordinates are sufficient. Since the discrete symmetry is a rotation, among the three retained coordinates, a single one must be invariant under the rotation symmetry. Consequently, modulus of modes  $a_1$  or  $a_3$  which are invariant under the order-2 rotation symmetry must be retained. Let us arbitrarily choose the modulus of mode  $a_3$ . Among the three

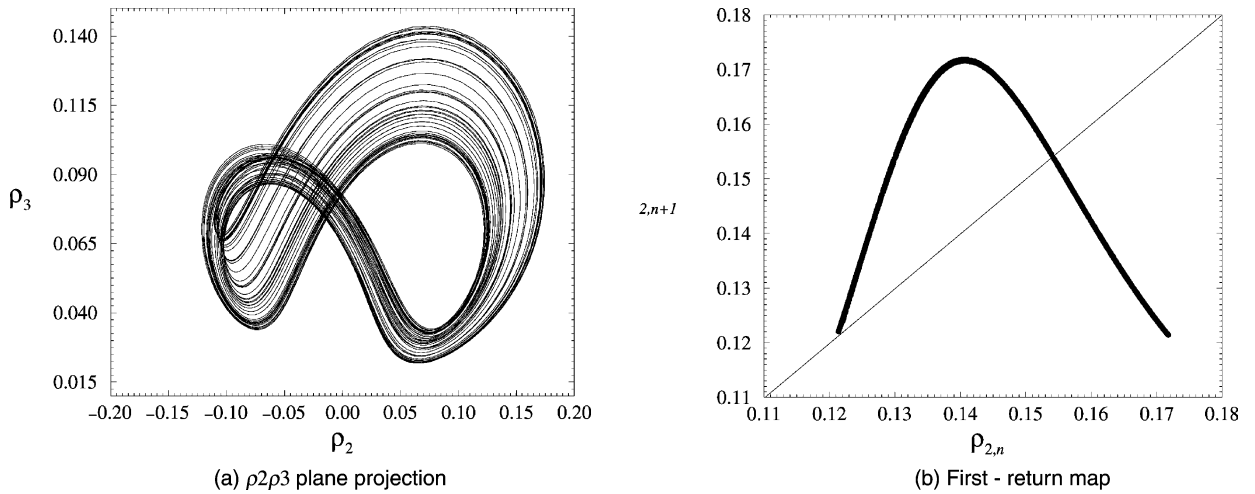


Fig. 6. Chaotic behaviour generated by the 10D system (4) and (5). The first-return map is a unimodal map with a differentiable maximum ( $v_1 = 0.050$ ,  $v_2 = -0.0345$ ,  $v_3 = 0.03$  and  $v_4 = 0.05$ ).

remaining modes, the modulus of  $a_2$  and  $a_4$  are chosen. Thus, the 3D space in which the topology of the attractor will be investigated is spanned by the coordinates  $(\tilde{\rho}_2, \tilde{\rho}_4, \rho_3)$ , where  $\tilde{\rho}_2$  and  $\tilde{\rho}_4$  designate the modulus of mode  $a_2$  and  $a_4$  for which the sign is varied in order to preserve the discrete rotation symmetry as discussed above. In the space  $\mathbb{R}^3(\tilde{\rho}_2, \tilde{\rho}_4, \rho_3)$ , the rotation is around the axis  $O\rho_3$ .

In that case, the image system is constructed with a nonlinear coordinate transformation  $(\tilde{\rho}_2, \tilde{\rho}_4, \rho_3) \mapsto (u, v, w)$  in which the coordinates  $(u, v, w)$  are invariant under the rotation symmetry  $\mathcal{R}_{\rho_3}(\pi)$ . The elementary polynomials in  $(\tilde{\rho}_2, \tilde{\rho}_4, \rho_3)$  of degree up to two, which are invariant under  $\mathcal{R}_{\rho_3}(\pi)$ , are  $\tilde{\rho}_2^2$ ,  $\tilde{\rho}_4^2$ ,  $\tilde{\rho}_2\tilde{\rho}_4$ ,  $\rho_3$  and  $\rho_3^2$ . The following coordinate transformation is convenient [14]:

$$\Psi \equiv \begin{cases} u = \Re(\tilde{\rho}_2 + i\tilde{\rho}_4)^2 = \tilde{\rho}_2^2 - \tilde{\rho}_4^2, \\ v = \Im(\tilde{\rho}_2 + i\tilde{\rho}_4)^2 = 2\tilde{\rho}_2\tilde{\rho}_4, \\ w = \rho_3. \end{cases} \tag{9}$$

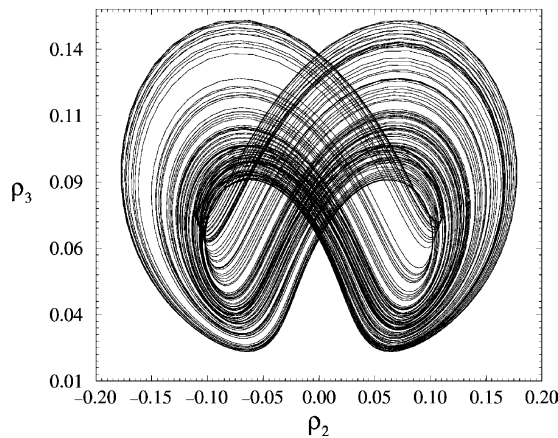


Fig. 7. Chaotic attractor globally invariant under the discrete rotation symmetry after the attractor merging crisis ( $v_2 = -0.0343$ ).

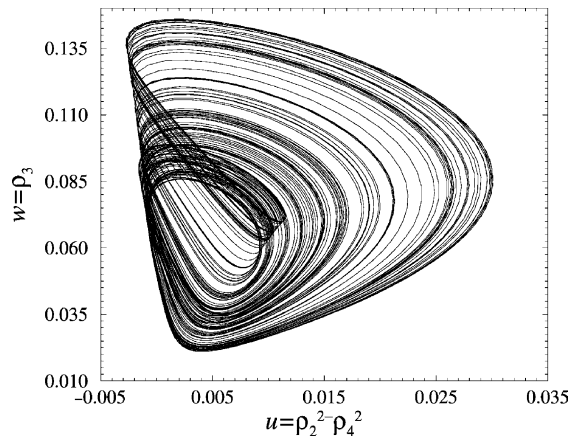


Fig. 8. Image of the chaotic attractor without any residual symmetry ( $v_2 = -0.0343$ ).

When this map is directly applied to the trajectory embedded within the phase space  $\mathbb{R}^3(\tilde{\rho}_2, \tilde{\rho}_4, \rho_3)$ , an image attractor without any residual symmetry (Fig. 8) is obtained. This image system is topologically equivalent to the attractor generated by the 8D model investigated in [6] but, it has the great advantage to be everywhere differentiable.

Let us start with one of the co-existing attractors in the phase space before the attractor merging crisis, that is, for  $v_2 > -0.0343$ . Since the first-return map is unimodal with a differentiable maximum, we should be able to synthesise the relative organisation of the periodic orbits embedded within the attractor by a branched manifold, a so-called template. A template is a knot-holder which synthesises all topological properties of unstable periodic orbits embedded within the attractor [7]. A first step may be to compute a first-return map to a Poincaré section as shown in Fig. 6b. In the present case, the first-return map is constituted by two monotonic branches, one increasing and one decreasing, split by a critical point C. An increasing (decreasing) branch is always associated with a stripe with an even (odd) number of half-turns. The template has therefore two stripes. The template is a Horseshoe template with a global torsion of a full turn (Fig. 9). In fact this template is equivalent to the one which characterises the attractor generated by the Lorenz system for  $R = 200$  ( $\sigma = 10$  and  $b = 8/3$ ). The template is then checked by computing the linking numbers from the extracted periodic orbits (see [10] for details). The fact that the topology of the attractor may be described by a template is a first confirmation evidence that the dynamics may be embedded within a 3D phase space.

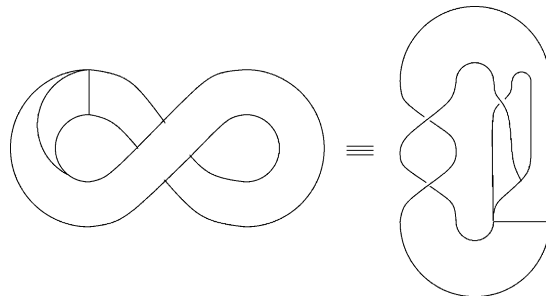


Fig. 9. Template of the chaotic attractor generated by the system (4) and (5) when the continuous symmetry is modded out. It is a Horseshoe template with a global torsion by a full-turn.

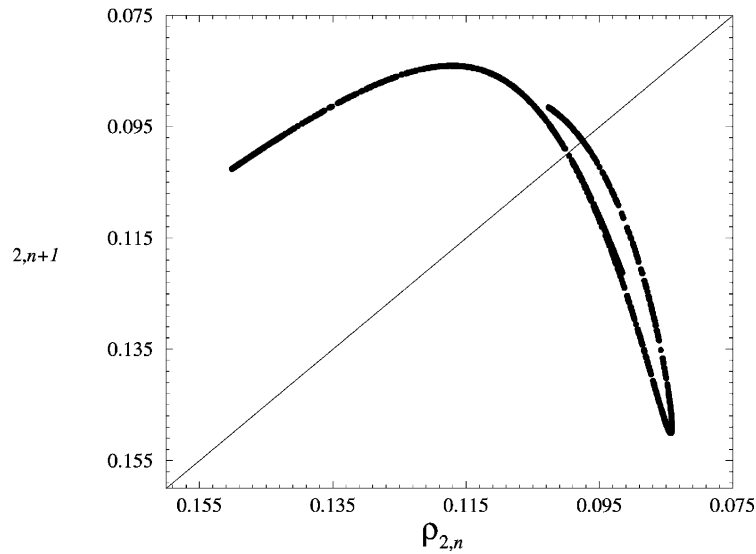


Fig. 10. First-return map to a Poincaré section of the image attractor ( $\nu_2 = -0.0343$ ).

When the parameter  $\nu_2$  is increased slightly, an attractor merging crisis is observed. The two attractors which co-exist in the phase space touch an unstable periodic orbit and become a single chaotic attractor that remains globally unchanged under the order-2 discrete symmetry (Fig. 7). Such a feature is also observed for the Lorenz system and the Burke and Shaw system. This is a quite common scenario for equivariant systems [12,21].

The topological analysis is then performed as usually for systems without any symmetry properties. The first-return map to a Poincaré section (Fig. 10) is a unimodal map with a differential maximum. As previously observed, the template has therefore one stripe with an even number of half-turns and one stripe with an odd number of half-turns. In fact, the template is similar to the one shown in Fig. 9. The main difference is in the population of periodic orbits. For  $\nu_2 = -0.0343$ , the dynamics is very close to the attractor merging crisis and, in that case, the symbolic dynamics is complete, that is, any possible sequence of “0” and “1” is realised as a periodic orbit within the attractor. For the symmetric attractor ( $\nu_2 = -0.0345$ ), the symbolic dynamics is pruned and, some symbolic sequences are realised as orbit within the attractor. The population of orbits with periodicity less than 9 is reported in Table 1 for the attractor after the attractor merging crisis.

### 3.3. 3D global models

One of the aims of this paper is to establish that the original dynamics, after modding out symmetries, can be correctly embedded in a 3D space. The means by which this will be accomplished is to search for global models

Table 1  
Population of orbits with periodicity less than 9 embedded within the chaotic attractor generated by the 10D model for  $\nu_2 = -0.0343^a$

1	101111	10111
10	10111110	10110
1011	10111111	1011010
10111010	1011111	1011011
101110	1011110	

<sup>a</sup> Some possible symbolic sequences are not realised as orbit embedded within the attractor; the symbolic dynamics is therefore pruned.

obtained directly from the original data without symmetries. If such models correctly reproduce the original dynamics and are 3D then the initial hypothesis is established. This section briefly reviews the modelling techniques used to obtain two global models that correctly represent the original dynamics without the continuous rotation symmetry. These models, which are very simple due to careful structure selection, commend themselves for simulation and analysis of the original image system. The models differ in the coordinate set on which they are built. One is built on delay coordinates and is a discrete-time model and the second is based on derivatives and is a continuous-time model. Both are 3D.

Since it is very likely that the dynamics may be embedded within the space  $\mathbb{R}^3(\tilde{\rho}_2, \tilde{\rho}_4, \rho_3)$ , the evolution of the system may be defined by a multivariate time series involving these three coordinates. It is thus desired to obtain a dynamical model from that multivariate time series with no prior knowledge, that will represent the original dynamics in some sense. In the remainder of this section, the NARMA model and the continuous-time model representations will be briefly reviewed, respectively. Such representations will be used on the multivariate time series to obtain 3D models for the attractor when the continuous rotation symmetry is modded out.

Here it is considered that the measured multivariate time series is  $\mathbf{x}_k = (x_k, y_k, z_k) (kT_s), k = 0, 1, \dots$  and where  $T_s = 0.2$  s is the sampling time. In many cases, the time evolution of the observed multivariate time series can be described by NARMA model [8] of the form

$$\begin{aligned} x_k &= F_x^\ell[\mathbf{x}_{k-1}, \dots, e_{x,k-1}, \dots, e_{x,k-10}], & y_k &= F_y^\ell[\mathbf{x}_{k-1}, \dots, e_{y,k-1}, \dots, e_{y,k-10}], \\ z_k &= F_z^\ell[\mathbf{x}_{k-1}, \dots, e_{z,k-1}, \dots, e_{z,k-10}]. \end{aligned} \quad (10)$$

Moreover, the multivariate time series is the output time series and  $e_{i,k}$  accounts for uncertainties, possible noise, unmodelled dynamics in each time series.  $F_i^\ell[\cdot]$  is some nonlinear function of  $\mathbf{x}_k$  and  $e_{i,k}$ . This model representation was chosen because it has shown to be adequate to represent, in compact form, a number of systems with chaotic dynamics [25].

In this paper, the map  $F_i^\ell[\cdot]$  is a polynomial of degree  $\ell \in \mathbb{Z}^+$ . In order to estimate the parameters of this map, each function in Eq. (10) can be expressed in the following form:

$$x_k = \boldsymbol{\psi}_{k-1}^T \hat{\boldsymbol{\theta}} + \xi_k, \quad (11)$$

where  $\xi_k$  are the identification residuals. Moreover,  $\boldsymbol{\psi}_{k-1}$  is a vector which contains output and residual terms up to and including time  $k-1$  and  $\hat{\boldsymbol{\theta}}$  is the estimated parameter vector obtained by minimising the following cost function [26]:

$$J_N(\hat{\boldsymbol{\theta}}_i) = \frac{1}{N} \sum_{k=1}^N \xi_{i,k}^2(\hat{\boldsymbol{\theta}}_i), \quad i = x, y, z \quad (12)$$

independently for each function  $F_i$ : Eq. (10) includes a moving average (MA) part composed of residual terms. This is done to significantly reduce parameter bias during estimation, however *only the deterministic part*, composed by the terms in  $x_k, y_k$  and  $z_k$  are used in the simulation and analysis. Because the residuals can only be calculated after all the model parameters have been estimated, Eq. (10) is “pseudo linear-in-the-parameters” and an iterative algorithm must be used. In fact, the extended least square algorithm can be used to successfully estimate the model parameters in the presence of the MA part of the model, which should be used, as explained before, to reduce bias on the parameters of the NAR part, which is the deterministic part of the model.

Parameter estimation is usually performed for a pseudo linear-in-the-parameters orthogonal model which is closely related to (11) and which is represented as

$$x_{i,k} = \sum_{j=1}^{n_p+n_\xi} g_j w_{j,k} + \xi_{i,k}, \quad (13)$$

where  $n_p + n_\xi$  is the number of (process plus noise) terms in the model,  $\{g_i\}_{i=1}^{n_p+n_\xi}$  are parameters and the monomials  $\{w_{j,k}\}_{j=1}^{n_p+n_\xi}$  are orthogonal over the data records. Finally, parameters of the model in Eq. (11) can be calculated from the  $\{g_j\}_{j=1}^{n_p+n_\xi}$ . This procedure has two major advantages, namely: (i) reduces inaccuracies due to numerical ill-conditioning; (ii) aids in selecting the structure of the final model. This last step is known to be a critical issue in nonlinear model building because a wrong structure does not only have *numerical* consequences but also *dynamical*. An incorrect structure does in fact induce spurious dynamics in the model.

A criterion for selecting the most important terms in the model can be devised as a by-product of the orthogonal parameter estimation procedure. The reduction in the mean square prediction error (MSPE) due to the inclusion of the  $j$ th term,  $g_j w_{j,k}$ , in the auxiliary model of Eq. (13) is  $(1/N)g_j^2 \bar{w}_{j,k}^2$ . Expressing this reduction in terms of the total MSPE yields the error reduction ratio (ERR) [26]:

$$[\text{ERR}]_j = \frac{g_j^2 \bar{w}_{j,k}^2}{\bar{x}_k^2}, \quad j = 1, 2, \dots, n_p + n_\xi. \quad (14)$$

Hence those terms with large values of ERR are selected to form the model.

Our objective is to obtain a 3D model to show that the dynamics underlying the 10D model when the continuous rotation symmetry is modded out may be reproduced by a 3D model (at least for certain parameter values). Using the notation  $(x, y, z) = (\tilde{\rho}_2, \tilde{\rho}_4, \rho_3)$  for simplification, the obtained model is

$$\begin{aligned} x_k &= 1.0680x_{k-1} + 3.1203y_{k-1}z_{k-1} - 0.074266x_{k-1}z_{k-1}^2 - 0.020243y_{k-1} - 8.6382x_{k-1}y_{k-1}^2 \\ &\quad - 0.1078x_{k-1}z_{k-1} + 2.119y_{k-1}z_{k-1}^2 - 4.7524y_{k-1}^3 - 0.4463x_{k-1}^2y_{k-1}, \\ y_k &= -0.0055474x_{k-1} + 0.95083y_{k-1} - 1.242x_{k-1}z_{k-1} - 1.1934y_{k-1}z_{k-1} + 1.8317x_{k-1}^3 \\ &\quad + 6.7074x_{k-1}^2y_{k-1} + 40.117x_{k-1}y_{k-1}^2 + 0.59054x_{k-1}z_{k-1}^2 + 38.189y_{k-1}^3, \\ z_k &= +0.94249z_{k-1} - 0.020179x_{k-1}^2 - 2.19x_{k-1}y_{k-1} - 0.61578y_{k-1}^2 + 0.10749z_{k-1}^2 + 0.43031x_{k-1}^2z_{k-1} \\ &\quad - 0.31945y_{k-1}^2z_{k-1} - 0.52538z_{k-1}^3 + 2.0311x_{k-1}y_{k-1}z_{k-1}, \end{aligned} \quad (15)$$

where  $x_k$ ,  $y_k$  and  $z_k$  designate the values of the variables  $x$ ,  $y$  and  $z$  at the discrete time  $k$ , respectively. In this representation, the time scale has been normalised with respect to the sampling time  $T_s$ , that is, the instant  $k-1$  refers to a time  $T_s$  prior to  $k$ . The residual terms are not shown since they are not used in the simulation. They were included, however, during parameter estimation to reduce bias. The model was obtained from a multivariate (three) time series with 1500 observations each corresponding to the 3D embedding shown in Fig. 7, that is, for  $\nu_2 = -0.0343$ . Note that all the monomials retained in the NARMA model satisfy the requirement for the rotation symmetry around the  $z$ -axis, that is, the monomials  $x^i y^j z^k$  are such as  $i+j$  are odd for the first two functions defining  $x_k$  and  $y_k$ . In the third function,  $i+j$  is even. These monomials have been automatically selected by the ERR structure selection, enforcing the rotation symmetry.

### 3.4. Topological validation of the 3D model

One may remark that the discrete-time model (15) is equivariant under a map  $\gamma : (x_k, y_k, z_k) \mapsto (-x_k, -y_k, z_k)$  defining an order-2 discrete rotation symmetry  $\mathcal{R}_z(\pi)$ . Iterating this global model allows to obtain a chaotic attractor (Fig. 11) which is topologically equivalent to the attractor generated by the 10D model when the continuous rotation symmetry is modded out. The topological validation is performed for the image representation of the model attractor obtained by applying the coordinate transformation  $(u, v, w) = (x^2 - y^2, 2xy, z)$ .

To give few elements, the first-return map to a Poincaré section for the NARMA model attractor (Fig. 12) is very similar to the one computed for the original dynamics (Fig. 10). The population of periodic orbits embedded

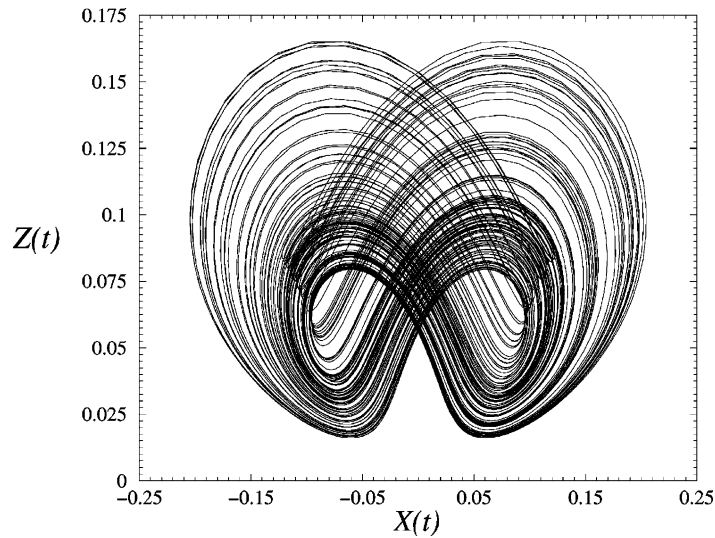


Fig. 11. Chaotic attractor obtained by iterating the identified NARMA model. This chaotic attractor is equivalent to the original one shown in Fig. 7.

within the model attractor is the same as the one reported in Table 1. Linking numbers for couples of periodic orbits have been computed and found in agreement with those predicted from the template shown in Fig. 9. The NARMA model reproduces therefore correctly the attractor shown in Fig. 7. Once the continuous symmetry is modded out, the underlying dynamics can therefore be embedded within a 3D phase space (at least for certain parameter values).

It has been recently shown that sometimes the bifurcation diagram may be partially reproduced from a model estimated from a time series recorded for a single value of the parameter [27,28]. Such a feature is successfully verified for the 3D NARMA model when the first monomial  $1.068x_{k-1}$  is replaced with  $\mu x_{k-1}$ . Thus, when the

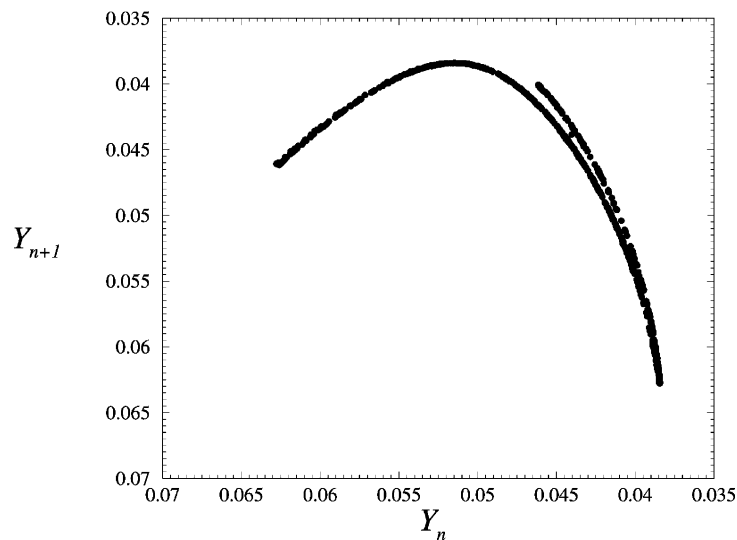


Fig. 12. First-return map to a Poincaré section of the chaotic attractor generated by the NARMA model (15).

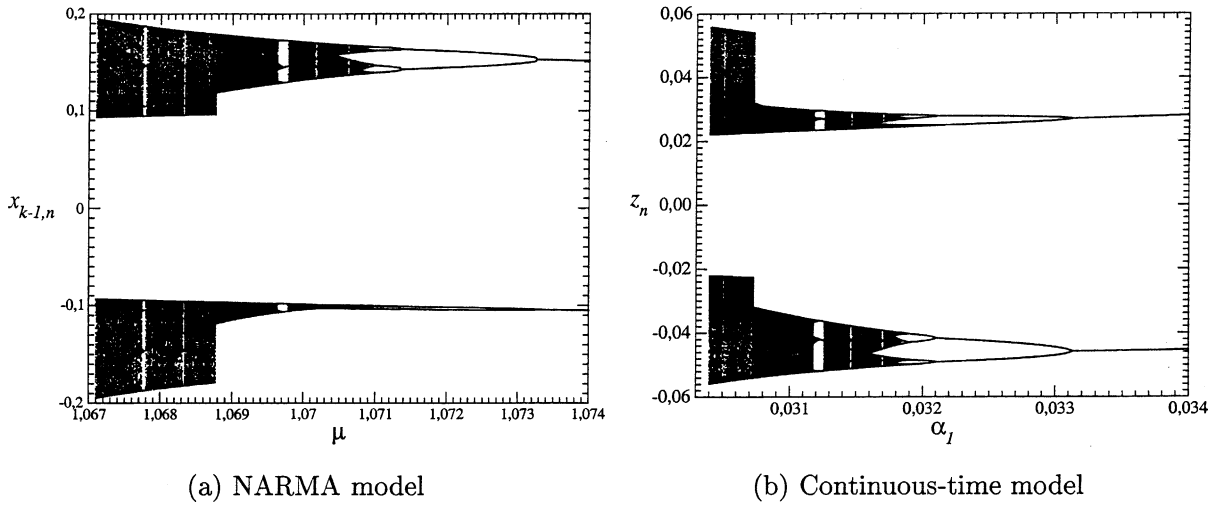


Fig. 13. Bifurcation diagram computed from the NARMA model (a) vs. the coefficient  $\mu$  when the first monomial  $1.0680x_{k-1}$  of system (15) is replaced with  $\mu x_{k-1}$ . The diagram associated with the continuous-time model (b) is computed vs. the parameter  $\alpha_1$ . Both models provide the same bifurcation diagram. There is no direct correspondence between  $x_{k-1}$  and  $z$ , since the models have very different structure. Only the dynamics may be compared.

$\mu$ -parameter is varied over the interval  $[1.067; 1.074]$ , a part of the bifurcation diagram is reproduced (Fig. 13a). The coefficient  $\mu$  may only be varied over the previous interval. When  $\mu < 1.067$ , the trajectory is ejected to infinity. Roughly, when the parameter  $\mu$  is decreased, a pitchfork bifurcation occurs and two period-1 limit cycles co-exist in the phase space. Both are simultaneously destabilised by a period-doubling bifurcation and two simultaneous period-doubling cascades are observed. Chaotic behaviours are then observed with the exception of periodic windows for few  $\mu$ -parameter values. Hereafter, an attractor merging crisis is observed for  $\mu \approx 1.0688$  and a single symmetric attractor is observed. This is exactly the bifurcation which is observed for the 3D embedding obtained when only the continuous rotation symmetry is modded out.

Similar results are obtained using a differential model representation. In that case, the continuous-time model has the form of the three ordinary differential equations

$$\dot{x} = F_x(x, y, z), \quad \dot{y} = F_y(x, y, z), \quad \dot{z} = F_z(x, y, z) \tag{16}$$

which are estimated independently on multivariate polynomial basis using a least-square method [9]. A simple structure selection based on the expected symmetry properties for the phase portrait shown in Fig. 7 is applied. Thus, since an order-2 rotation around the  $z$ -axis is expected, the monomials  $x^i y^j z^k$  must satisfy  $i + j$  odd for the first two functions  $F_x$  and  $F_y$ , and  $i + j$  even for the third one. Once the model is obtained, a second structure selection is applied by hand: nine terms which do not affect the dynamics were removed. The lack of effect on the dynamics was determined by the large variations of their values observed when the modelling parameters are slightly changed. The model then reads as

$$\begin{aligned} \dot{x} &= \alpha_1 x + \alpha_2 y z + \alpha_3 x^3 + \alpha_4 x^2 y + \alpha_5 x y^2 + \alpha_6 y z^2, \\ \dot{y} &= \beta_1 x + \beta_2 y + \beta_3 x z + \beta_4 y z + \beta_5 x^3 + \beta_6 x^2 y + \beta_7 x y^2 + \beta_8 x z^2 + \beta_9 y z^2, \\ \dot{z} &= \gamma_1 z + \gamma_2 x y + \gamma_3 x y z \end{aligned} \tag{17}$$

for which the coefficients are reported in Table 2. Similarly to the NARMA model, this continuous-time model generates a chaotic attractor which is topologically equivalent to the original dynamics when the continuous rotation

Table 2

Coefficients of the three ordinary differential equations obtained for the 3D differential model obtained when the continuous rotation symmetry is modded out

$i$	$\alpha_i$	$\beta_i$	$\gamma_i$
1	0.03040	−0.00331	−0.03001
2	1.69058	−0.03728	−0.99819
3	−0.08304	−0.64343	−0.03534
4	−0.26199	−0.27072	
5	−2.14262	0.66183	
6	0.69238	0.59883	
7		10.6746	
8		1.08209	
9		1.36005	

is modded out. When the parameter,  $\alpha_1$ , is varied, a bifurcation diagram similar to the one obtained for the NARMA model is computed (Fig. 13b). Both approaches thus provide similar features. The 3D character of the dynamics is thus confirmed.

Further support for model validation comes from the Lyapunov exponents (Table 3). Indeed, the largest exponent  $\lambda_1$  is in good agreement between the original 10D dynamics and the two 3D models. This shows that quantitative dynamical characteristics such as entropy are also recovered by the models. One may also note that the Lyapunov dimension computed from the standard Kaplan–Yorke formula agrees well for the discrete and continuous models, respectively, 2.05 and 2.04. For the 10D system, the continuous rotation symmetry induces two vanishing exponents which increase the dimension by two with respect to the situation where this continuous symmetry is modded out. For instance, a dimension of 4.10 is estimated, which corresponds rather well to the dimension of the 3D models increased by two.

### 3.5. Comparison with the Lorenz dynamics

When only the continuous rotation symmetry is modded out, the dynamics of the nonlinear wave–wave interactions model is very similar compared to those generated by the Lorenz system:

$$\dot{x} = -\sigma x + \sigma y, \quad \dot{y} = Rx - y - xz, \quad \dot{z} = -bz + xy \quad (18)$$

for  $(R, \sigma, b) = (198, 10, 8/3)$ . The chaotic attractor thus generated is globally unchanged under the rotation symmetry  $\mathcal{R}_z(\pi)$  of the Lorenz system (Fig. 14). For the parameter values chosen, the attractor is located just after an attractor merging crisis when  $R$  is decreased. Such a feature already ensures that the dynamics will have certain properties similar to those observed for the original attractor.

As for the original dynamics and the NARMA model, the image system is built for the topological analysis. The corresponding attractor (Fig. 15) looks slightly different. This results from an orientation of the 3D embedding in the phase space  $\mathbb{R}^3(\tilde{\rho}_2, \tilde{\rho}_4, \rho_3)$  (Fig. 7) which is slightly different than the orientation of the Lorenz attractor

Table 3

First five Lyapunov exponents computed for the original 10D system and the three exponents of the 3D models<sup>a</sup>

	$\lambda_1$	$\lambda_2$	$\lambda_3$	$\lambda_4$	$\lambda_5$
10D	0.0039	$1 \times 10^{-6}$	$8 \times 10^{-7}$	$2 \times 10^{-7}$	−0.039
3D NARMA	0.0041	$-8 \times 10^{-8}$	−0.0737	–	–
3D continuous	0.0038	$-3 \times 10^{-7}$	−0.0830	–	–

<sup>a</sup> Note that for the 10D model three components can be considered as zero within the numerical precision of the computation.

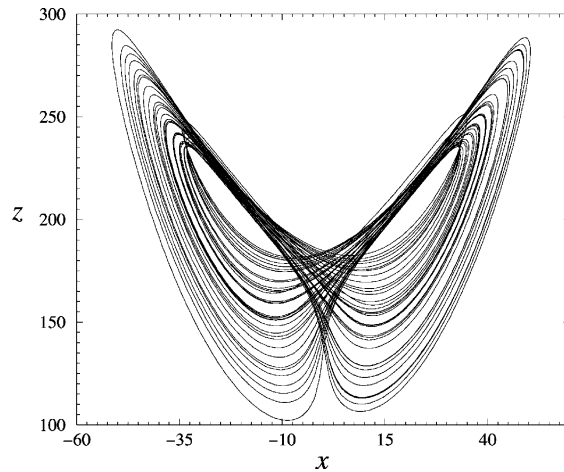


Fig. 14. Chaotic attractor generated by the Lorenz system which is topologically equivalent to the dynamics generated by the 10D model when the continuous rotation is modded out.  $(R, \sigma, b) = (198, 10, 8/3)$ .

in the space  $\mathbb{R}^3(x, y, z)$ . Nevertheless, when the first-return map to a Poincaré section is computed (Fig. 16), this is a quite similar map which is recovered. Note that even the layered structure of the decreasing branch is also reproduced. The population of periodic orbits embedded within the attractor is the same than the one reported in Table 1. Moreover, the template characterising this attractor is also the template shown in Fig. 9. When the continuous rotation symmetry is properly modded out, that is, in preserving the discrete order-2 symmetry, the original dynamics is therefore topologically equivalent to the Lorenz attractor.

The bifurcation diagram versus the  $R$ -parameter value is computed (Fig. 17) which is similar to those previously computed (Fig. 13). This strongly suggests that the dynamics without the continuous rotation symmetry is of the Lorenz type, at least for certain parameter values and from a topological point of view.

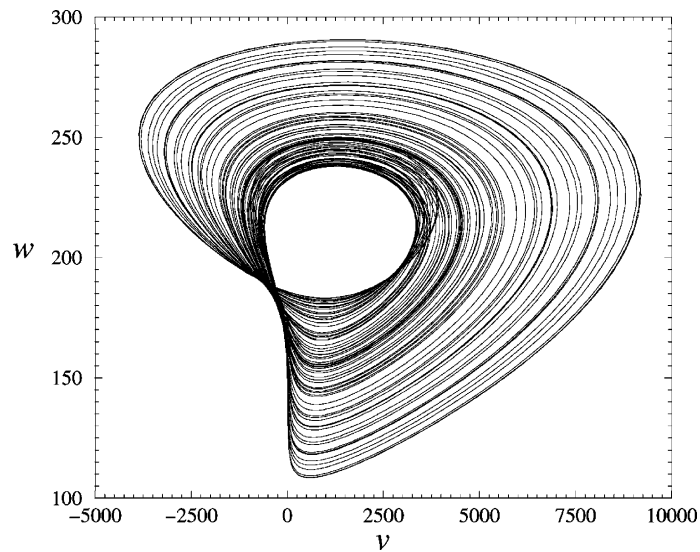


Fig. 15. Image attractor without any residual symmetry of the Lorenz system for  $(R, \sigma, b) = (198, 10, 8/3)$ .

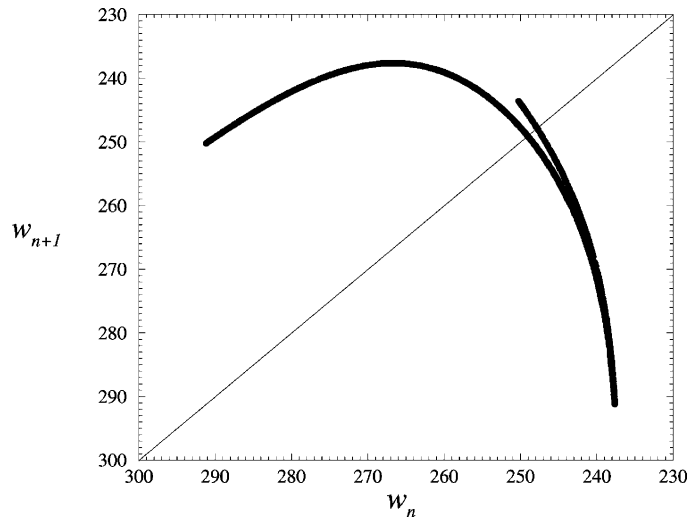


Fig. 16. First-return map of the chaotic attractor generated by the image of the Lorenz system  $(R, \sigma, b) = (198, 10, 8/3)$ .

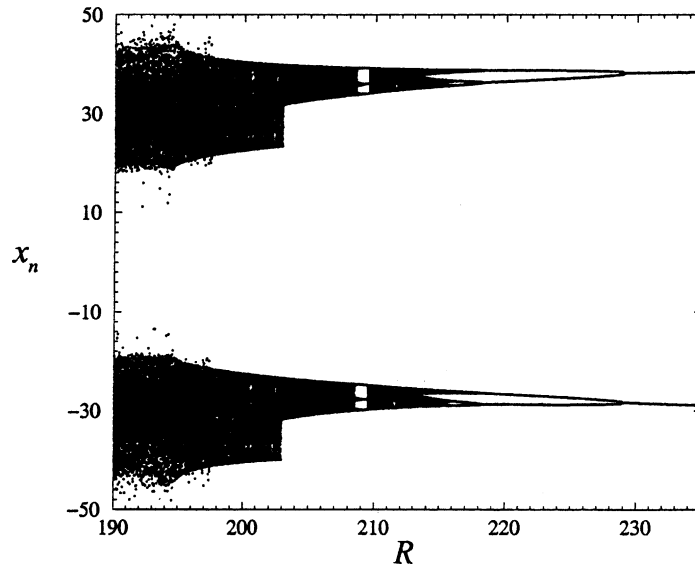


Fig. 17. Bifurcation diagram of the Lorenz system vs.  $R$  for  $(\sigma, b) = (10, 8/3)$ . A pitchfork bifurcation (not shown) occurs for  $R = 313.8$ . Each part of this diagram corresponds to one of the two wings of the Lorenz system.

#### 4. Conclusion

Although generated by a 10D model, the dynamics underlying interacting electrostatic waves is not necessarily too complicated. In particular, when the continuous rotation symmetry is modded out, the modified decay instability has a dynamics which is topologically equivalent to the Lorenz dynamics. This exhibits an unexpected analogy with a decay instability driven by a coherent pump wave which has an attractor of the Lorenz-type [29], at least for certain parameter values. This suggests that complex behaviours as observed when the continuous rotation symmetry is kept

may result from quite simple dynamics conjugated with more or less obvious symmetry properties. It is therefore relevant to be able to identify the possible symmetries which may be involved in the system under study. Indeed, this is an important step before attempting a global model from a time series since it is not possible to obtain a global model from the data where the continuous rotation symmetry is maintained. If this is true for numerical data, this will be reinforced for experimental data where the noise contamination is always an additional difficulty. This reveals that using symmetry properties for investigating dynamics may be very important.

It has been shown how the identification of symmetry properties, topological analysis and global modelling techniques may be used for investigating dynamics. All of these techniques may be used to investigate experimental dynamics. Taking into account the symmetry properties is useful to simplify the analysis. Sometimes it is not even possible to compare directly experimental dynamics and models because measurements naturally mod out the symmetries. This is the case when electromagnetic fields are involved and only the intensities are measured. Global modelling techniques can be used to obtain deterministic equations that capture the underlying dynamics. This is particularly convenient to prove that the data used to obtain the model are deterministic rather than stochastic. When only a small amount of data is available, it is possible to use the model to generate very long (stationary) time series and, consequently, to be able to perform an accurate dynamical analysis, such as topological analysis.

The analogy between the 10D model and the 3D Lorenz system is only valid for certain parameter values. Since it is known that modified decay instability behaves in a different way than the single decay instability [30–32], such analysis remains to be extended to a broader range but there is no doubt that this is already a helpful starting point for understanding the road from chaos to hyperchaos, that is, how a second Lyapunov exponent becomes positive. It is believed that the procedures and results discussed in this paper are relevant preliminary steps before investigating experimental dynamics.

## Acknowledgements

C. Letellier wishes to thank Robert Gilmore for helpful discussions. He and L. Aguirre thank CNPq and CNRS for supporting research collaboration. The authors are grateful to T. Dudok de Wit and V. Krasnoselskikh for stimulating discussions. B. Lefebvre acknowledges a postdoctoral fellowship from the CNES.

## References

- [1] P.A. Robinson, Nonlinear wave collapse and strong turbulence, *Rev. Mod. Phys.* 69 (1997) 507–573.
- [2] R.P. Lin, W.K. Levadal, W. Lotko, D.A. Gurnett, F.L. Scarf, Evidence for nonlinear wave–wave interaction in solar type III radio bursts, *Astrophys. J.* 308 (1986) 954.
- [3] G.B. Hospodarsky, D.A. Gurnett, Beat-type Langmuir wave emissions associated with a Type III solar radio burst: evidence of parametric decay, *Geophys. Res. Lett.* 22 (1995) 1161–1164.
- [4] I.H. Cairns, P.A. Robinson, Ion acoustic wave frequencies and onset times during Type III solar radio bursts, *Astrophys. J.* 453 (1995) 959.
- [5] S.D. Bale, D. Burgess, P.J. Kellogg, K. Goetz, R.L. Howard, S.J. Monson, Phase coupling in Langmuir wave packets: possible evidence for three-wave interaction in the upstream solar wind, *Geophys. Res. Lett.* 23 (1996) 109–112.
- [6] B. Lefebvre, V. Krasnosel'skikh, Nonlinear interaction of four electrostatic waves in a plasma, *Physica D* 152–153 (2001) 742–751.
- [7] R. Gilmore, Topological analysis of chaotic dynamical systems, *Rev. Mod. Phys.* 70 (4) (1998) 1455–1529.
- [8] I.J. Leontaritis, S.A. Billings, Input–output parametric models for nonlinear systems. Part II. Stochastic nonlinear systems, *Int. J. Contr.* 41 (2) (1985) 329–344.
- [9] G. Gouesbet, C. Letellier, Global vector field reconstruction by using a multivariate polynomial  $L_2$ -approximation on nets, *Phys. Rev. E* 49 (6) (1994) 4955–4972.
- [10] C. Letellier, P. Dutertre, B. Maheu, Unstable periodic orbits and templates of the Rössler system: toward a systematic topological characterization, *Chaos* 5 (1) (1995) 271–282.
- [11] V. Krasnosel'skikh, B. Lefebvre, T. Dudok de Wit, D. Mourenas, Synchronization vs. stochastization of phases in four-wave interaction, *Physica Scripta* 57 (1998) 246–252.

- [12] C. Letellier, P. Dutertre, J. Reizner, G. Gouesbet, Evolution of multimodal map induced by an equivariant vector field, *J. Phys. A* 29 (1996) 5359–5373.
- [13] C. Letellier, G. Gouesbet, Topological characterization of reconstructed attractors modding out symmetries, *J. de Physique II* 6 (1996) 1615–1638.
- [14] C. Letellier, R. Gilmore, Covering dynamical systems: two-fold covers, *Phys. Rev. E* 63 (2001) 16206.
- [15] E.N. Lorenz, Deterministic nonperiodic flow, *J. Atmos. Sci.* 20 (1963) 130–141.
- [16] V.E. Zakharov, Collapse of Langmuir waves, *Sov. Phys. JETP* 35 (5) (1972) 908–914.
- [17] V.V. Krasnosel'skikh, V.I. Sotnikov, Plasma-wave collapse in a magnetic field, *Sov. J. Plasma Phys.* 3 (4) (1977) 491–495.
- [18] V.E. Zakharov, S.L. Musher, A.M. Rubenchik, Hamiltonian approach to the description of non-linear plasma phenomena, *Phys. Rep.* 129 (1985) 285–366.
- [19] H.D.I. Abarbanel, M.B. Kennel, Local false nearest neighbors and dynamical dimensions from observed chaotic data, *Phys. Rev. E* 47 (5) (1993) 3057–3068.
- [20] L. Cao, Practical method for determining the minimum embedding dimension of a scalar time series, *Physica D* 110 (1/2) (1997) 43–52.
- [21] C. Letellier, J.M. Malasoma, Unimodal order in the image of the simplest equivariant jerk system, *Phys. Rev. E* 64 (2001) 067202.
- [22] M.J. Feigenbaum, Quantitative universality for a class of nonlinear transformation, *J. Stat. Phys.* 19 (1) (1978) 25–52.
- [23] P. Coullet, C. Tresser, Itérations d'endomorphismes et groupe de renormalisation, *J. de Physique, Colloque C5* 8 (39) (1978) C5–C25.
- [24] O.E. Röessler, Horseshoe map chaos in the Lorenz equations, *Phys. Lett. A* 60 (5) (1977) 392–394.
- [25] L.A. Aguirre, S.A. Billings, Retrieving dynamical invariants from chaotic data using NARMAX models, *Int. J. Bifurcat. Chaos* 5 (2) (1994) 449–474.
- [26] S. Chen, S.A. Billings, W. Luo, Orthogonal least squares methods and their application to nonlinear system identification, *Int. J. Contr.* 50 (5) (1989) 1873–1896.
- [27] E. Bagarinao, K. Pakdaman, T. Nomura, S. Sato, Reconstructing bifurcation diagrams from noisy time series using nonlinear autoregressive models, *Phys. Rev. E* 60 (1) (1999) 1073–1076.
- [28] L.A. Aguirre, C. Letellier, J. Maquet, Induced bifurcations in the validation of nonlinear dynamical models, *Int. J. Bifurcat. Chaos* 12 (1) (2002) 135–145.
- [29] A.S. Pikovsky, M.I. Rabinovich, V.Yu. Traktengerts, Onset of stochasticity in decay confinement of parametric instability, *Sov. Phys. JETP* 47 (4) (1978) 715–719.
- [30] S.Ya. Vyshkind, M.I. Rabinovich, The phase stochasticization mechanism and the structure of wave turbulence in dissipative media, *Sov. Phys. JETP* 44 (1976) 292–299.
- [31] J.M. Wersinger, J.M. Finn, E. Ott, Bifurcation and “strange” behavior in instability saturation by nonlinear three-wave coupling, *Phys. Fluids* 23 (1980) 1142–1154.
- [32] D.W. Huges, M.R.E. Proctor, Chaos and the effect of noise in a model of three-wave mode coupling, *Physica D* 46 (1990) 163–176.